

# RESEARCH ARTICLE

# Numerical investigation on stress concentrations of circular steel Xjoints

Erdal Gül<sup>1</sup>, Zeynep Fırat Alemdar<sup>1</sup>

<sup>1</sup> Yıldız Technical University, Department of Civil Engineering, Istanbul, Türkiye

## **Article History**

Received 6 November 2023 Accepted 16 February 2024

## Keywords

X-type brace Stress concentration Finite element Weld thickness Connection plate

#### **Abstract**

The most important reasons for the usage of steel as a building material are its high strength and ductile behavior, which can be defined as inelastic deformation or displacement capacity under a certain load. Steel frames are required to sustain the horizontal loads during an earthquake. The steel frames are classified as momentresisting steel frames, concentric steel braced frames, eccentric braced steel frames, and buckling restrained braced frames. These steel frames can be designed with a high ductility level frame, limited ductility level frames, and ductility level mixed frames. In this study, stress concentrations due to the maximum compression force that may occur during an earthquake have been examined by the finite element method at the connection point of the circular cross-sectional braces of the central X-type braced steel frame with a high ductility level. Stress concentrations in the Xtype brace were investigated depending on the variation of the cut surface required for the connection plate due to the change in the angle between the braces and the differences in the weld thickness applied in this region. In the models, the angle between the braces is designed as 60°, 75°, and 90° and the weld thicknesses are defined as 3.5 mm, 5 mm, and 7 mm. The results are obtained by applying the same compressive and tensile forces to the braces under the same boundary conditions and compared for these different models. It is obtained that the highest stress values occur along the direction of the tensile force in the tension profile and nearly at a distance of 5 mm after the cut. The maximum stress values decrease when the intersection angle between the braces increases from 60° to 90°.

### 1. Introduction

Although many natural disasters are encountered in the world, earthquakes are one of the most devastating natural hazards for human life. The main reason why a natural event turns into a natural disaster is that a large part of the existing structures did not receive any engineering service. Due to the damage and collapse of most reinforced concrete structures that occurred in the Marmara and Duzce earthquakes in 1999, the usage of steel material has been increased and the section about steel structures in the 2007 Turkish Earthquake Code was reviewed and improved [1]. Thus, the Design, Calculation, and Construction Principles of Steel Structures (SDCCSS, 2018) [2] and the Turkish Building Earthquake Code (TBEC, 2019) [3] have reached the initial stages.

eISSN 2630-5763 © 2023 Authors. Publishing services by golden light publishing®.

<sup>\*</sup> Corresponding author (<u>zalemdar@yildiz.edu.tr</u>)

Steel is used as a construction material in many types of buildings since the strength and elasticity modulus of the material are very high compared to other materials and the construction time is fast. Most of these structures are single-story or several-stories, used for workshops and factories, and about 60% of them are industrial steel structures. It consists of portal frame systems or truss beam systems resting on fixed base columns in one direction and braced shear wall systems in the other direction [4]. Due to the increasing usage of steel structures, it is important to examine and develop steel materials, members, and systems.

Steel frame systems can generally be divided into two main classes: moment-resisting frame systems and braced frame systems. Braced steel frame systems are classified as special concentrically braced frames, concentrically braced frames, eccentrically braced frames, and buckling restrained braced frames [5]. Steel braces are used to increase the horizontal load-carrying capacity of structures and reduce lateral drift. Concentrically braced steel frame systems can be designed as systems with a high level of ductility to seriously prevent loss of strength throughout the structure under the effect of an earthquake. The energy resulting from the horizontal loads acting on the system is consumed by the cross members and should be designed so that one carries compression forces while the other works for tension [6]. Brace members must be designed to meet the compression forces of at least 30% and at most 70% of the horizontal forces acting in both earthquake directions [3].

Many analytical and experimental studies have been conducted on steel braces. Bosco and Rossi analytically examined the seismic behavior of structures with eccentric supports in dual systems consisting of eccentrically supported frames and moment-resisting frames, by following the force design approach and capacity design principles [7]. Turker and Lekesiz examined the earthquake performances of different braced shear wall alternatives in steel industrial buildings designed according to the TBEC-2007 [8]. Earthquake performances of concentrically braced steel frames designed according to TBEC-2007 and ASCE-7 were examined using nonlinear time history analysis [9]. Two buildings with 3 and 9 floors were examined under 5 severe earthquake records and the increased earthquake loading criterion in TDY-2007 was evaluated.

The earthquake performances of single-story steel industrial buildings designed according to the TBEC-2007 and the stability problems affecting the earthquake performances were examined [10]. The load-bearing systems of the buildings are composed of frame systems with inclined beams or lattice beams in one direction, and shear wall systems with concentrically braced steel frames in the other direction. Performance criteria and modeling parameters recommended in ASCE/SEI 41-06 were used in the performance evaluations of buildings. The life safety performance level predicted in TBEC-2007 was achieved under the design earthquake in almost all building load-bearing systems examined.

The effect of different bracing arrangements in concentrically braced steel frames (CBSF) on the earthquake performance of the frame was examined in detail by nonlinear dynamic time history analysis. In the study, X and inverted V diagonal frames were examined [11]. The earthquake performances of both X-braced and inverted V-braced frames were obtained very close to each other.

During a severe earthquake, the braced members in the concentrically braced frame are subjected to large deformations in cyclic tension or compression loads in the post-buckling region. In order for these frames to survive such large repetitive deformations without early collapse, the brace members and their connections must be properly detailed. It has been shown that the damage of concentrically braced frames observed during past earthquakes and laboratory tests is mostly due to brittle fractures and limited ductility resulting from the failure of brace members or connection elements [1]. Concentrically braced frame members are exposed to large local buckling at low-story drifts, with their effects decreasing in the nonlinear region. Large story drifts resulting from early failure of the brace member require the columns, beams, and connections in the system to be very ductile.

Within the scope of this study, stress concentrations caused by the discontinuity in the profile crosssection formed due to the connection of the X-type brace were evaluated by varying the angle between the

X braces and the thickness of the weld between the tension brace and the connection plate. Detailed finite element models of the X brace connections were created using the ANSYS program [12] and the results were compared for different cases.

#### 2. The finite element models of the connections

### 2.1. Geometry

The circular cross-sectional X-type brace members and the connection plate were modeled in accordance with the connection shown in Fig. 1. The outer diameter of the circular profile cross-section was taken as 127 mm and the thicknesses of the profiles and the plates were selected as 10 mm.

In Article 13.2.2.2 titled "Limitations" in the SDCCSS-2018 [2], it is stated that the minimum thickness for the fillet welds should be taken as 3.5 mm if the wall thickness (t) of the thinner members in the connection is between 6 and 13 mm. In the models, the thickness of the members is 10 mm, thus the minimum weld thickness is chosen as 3.5 mm. In addition, since the maximum weld thickness can be taken as 0.7\*t according to the Specification, the maximum weld thickness was taken as 7 mm. Thus, nine different FE models were created by defining the weld thicknesses as 3.5 mm, 5 mm, and 7 mm in the middle part of the tension profile, which is about 500 mm long, and changing the angle between the braces as 60°, 75° and 90°. The weld thickness was taken as 3.5 mm in the other parts of the connections.

In the FE program, four elements forming the lower and upper compression profiles were designed using Solid187 type tetrahedral element, and the other elements were designed using Solid186 type hexahedral element as shown in Fig. 2. The tension profile was divided into three regions as upper, lower and middle parts, and the compression profile was divided into two regions, upper and lower, due to the connection of the braces. The length of the tension profile and the distance between the upper and lower points of the compression profile were kept constant for each model and accepted as 6,000 mm.

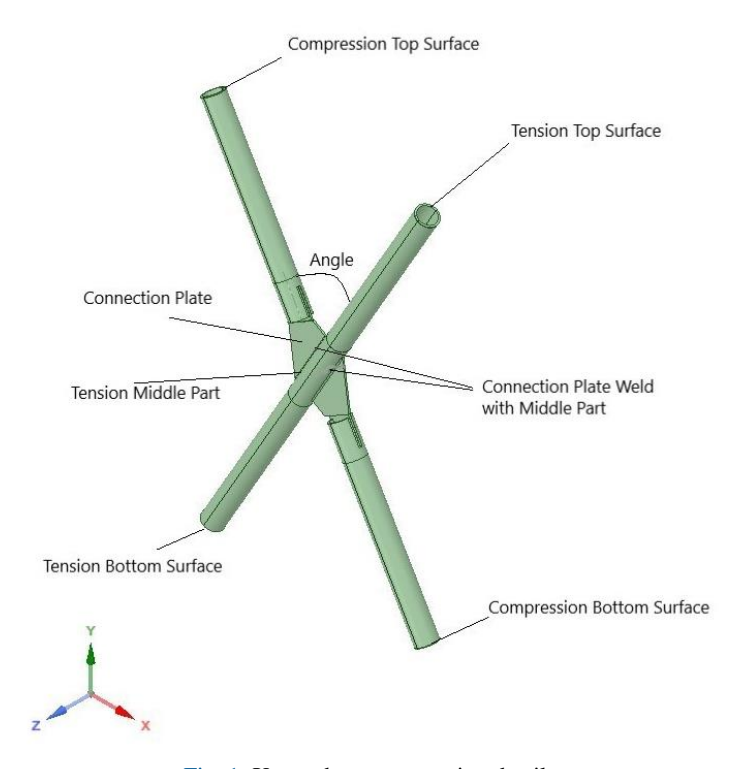


Fig. 1. X-type brace connection details

Surface interactions on the connection plate, the tension profile, and the compression profile were defined. Interaction types were selected as "no separation" for areas that are allowed to move on each other, and "bonded" for surfaces either welded or the whole part. The model was separated into finite elements, which would directly affect the analysis results. Within the scope of this study, since the part where the stress distribution is investigated is the middle part of the tension profile, the surface mesh size along the part was set to 5 mm in Fig. 2. The dimension of the mesh along the cross-section of the profiles was defined as 2.5 mm to obtain four equal sizes of finite elements as shown in Fig. 3. The mesh size along the weld was set to 2.5 mm. In other parts of the model, the dimension of the mesh was taken as 10 mm. The total number of finite elements in the models was kept around 105,000 as shown in Fig.2.

The cut surfaces formed in the top surface of the tension profile are called "1. Surface" which is the small surface at the top, "2. Surface", the other small surface at the opposite, "3. Surface" which is the long surface on the left, and "4. Surface", the long surface on the right, as shown in Fig. 4. Similarly, the cut surfaces on the bottom surface corresponding to those described in the top surface are defined as "5. Surface", "6. Surface", "7. Surface", and "8. Surface", respectively, in Fig. 5. The location of the surfaces is important in understanding where the stress is concentrated.

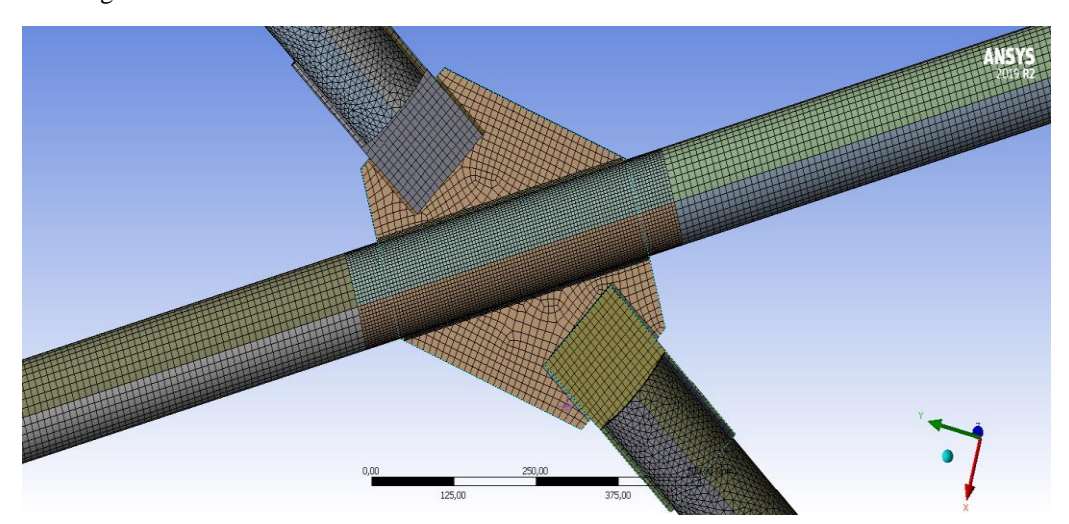


Fig. 2. Mesh details of the connection

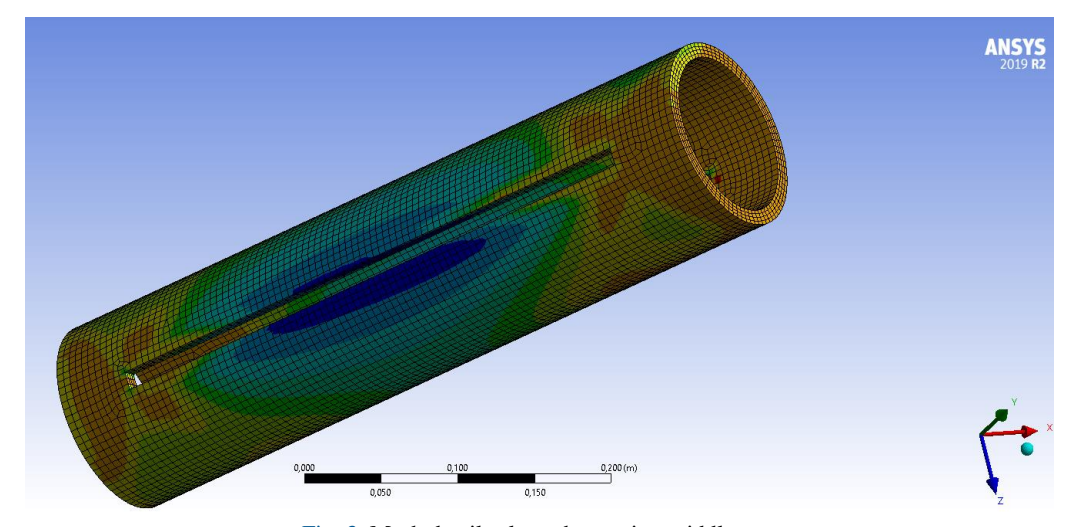


Fig. 3. Mesh details along the tension middle part

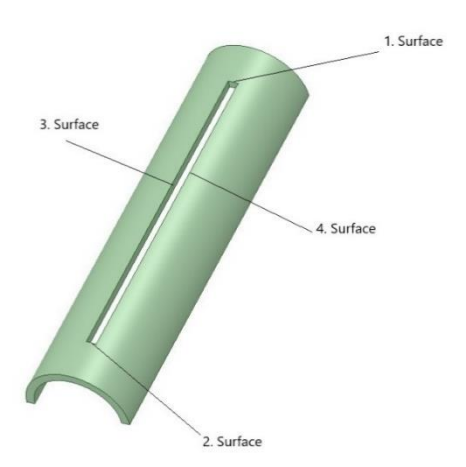


Fig. 4. Tension profile top surfaces

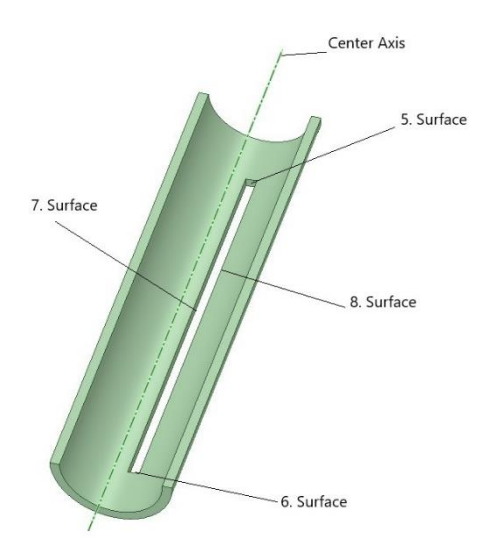


Fig. 5. Tension profile bottom surfaces

When the angle between the braces is taken as 60°, 75°, and 90°, the upper edge center point of the 4. The surface remained the same for all the models and the lengths given in Table 1 were changed according to this point. The reason why the length of the cut varies depending on the angle is that the two opposite sides of the connection plate connect with an angle of 30°, as shown in Figure 1. The middle part of the tension profile with a length of 250 mm to the left and right of the center point of the profile is investigated. Since the cut surface length varies between 322 and 396 mm depending on the angle change, a path with a 500 mm length was deemed to be sufficient. Stresses occurred following the cut surfaces were examined as well as the stresses within the cut surfaces.

The center points of the cut surfaces and the surfaces with the highest stress were taken into consideration as shown in Fig. 6 and Fig. 7. Three paths were defined to examine the results obtained from the FE models. The first path is called "Path-4" which is the line passing through the intersection of the 4. The surface and the outer face of the tension profile as shown in Fig. 6. The second path called "Path-5" is defined between the center point of 1. The surface and the end of the tension middle part as illustrated in Fig. 7. The third path called "Path-8" is drawn along the 8. The surface at the bottom surface of the tension profile is similar to the Path-4.

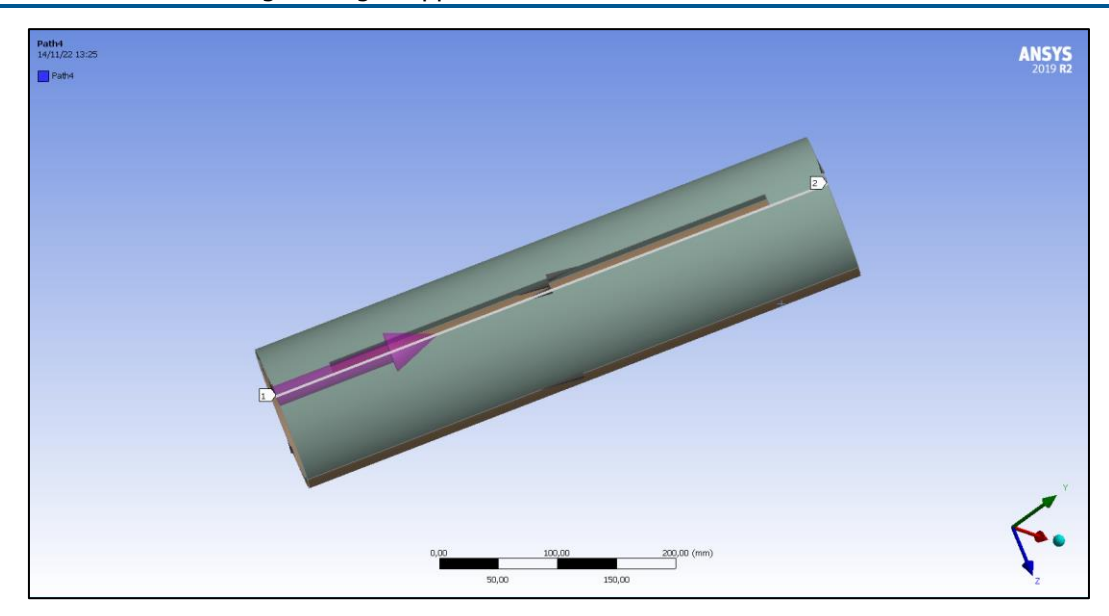


Fig. 6. Detail view of Path-4

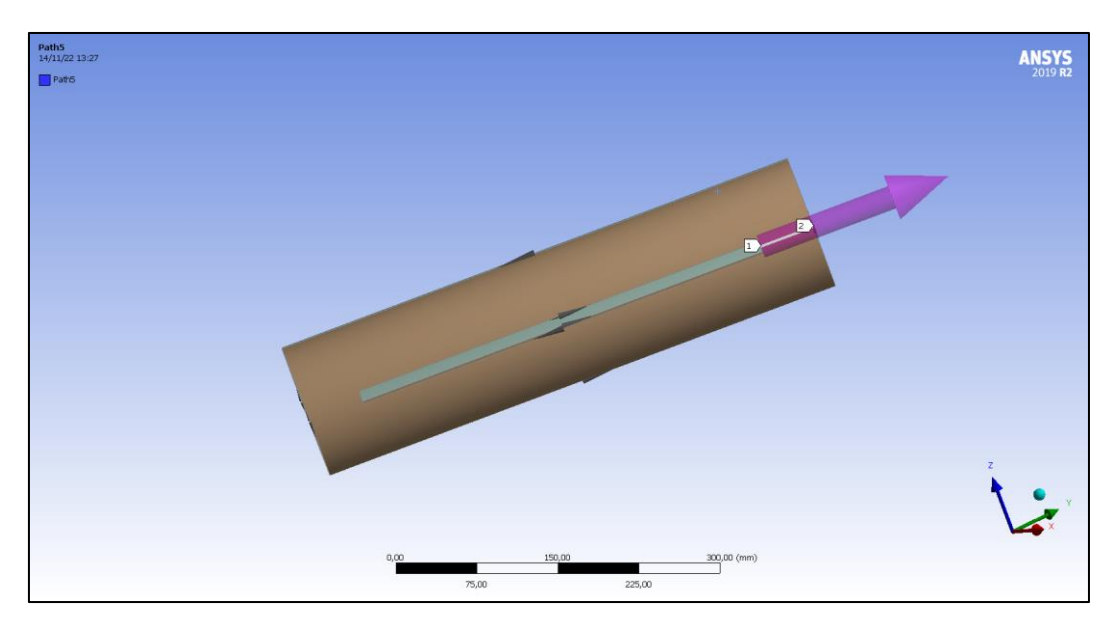


Fig. 7. Detail view of Path-5

Table 1. Length data based on the angle between X brace members

Angle	60°	75°	90°	60°
Length of cut in the middle of the tension profile (mm)	396	343	322	396
Absolute length from center point to cut surface (mm)	198	171	161	198
Side distance after cut surface (mm)	52	79	89	52

## 2.2. Material

In the connection models, S275 structural steel was chosen as the material type. Article 9.2 titled "Possible Material Strength" in TBEC [3] states the possible yield and tensile strengths of the selected material in steel

structures and connection elements instead of the yield and rupture strengths. The coefficients,  $R_y$  and  $R_t$  used in the calculation of the possible (expected) yield strength and the possible tensile strength are defined depending on the type of material. Based on S275 structural steel properties, the possible yield and tensile strengths are obtained as 385 MPa and 559 MPa for the circular profile and 357.5 MPa and 473 MPa for the plate. Additionally, the plasticity properties of steel are required to be defined. These properties can be described as multilinear isotropic if obtained through experimental studies, or as bilinear isotropic if there are no experimental studies. In this study, a bilinear isotropic curve was defined as a linear line up to the yield strength and then a broken line after the yield strength. The tangent modulus, which is the slope of the second broken line where the plastic behavior is determined, can be determined as 0.1%, 0.2%, 1%, and 16% of the elasticity modulus of steel. In the analysis of the models, the tangent modulus was taken as 2,000 MPa, accepted as 1% of the elasticity modulus for both the profile and the plate. For the material definition of the weld in the connections, the possible strength values for the steel material were utilized based on the requirements in Article 13.2.6 in the SDCCSS-2018 [2].

### 2.3. Boundary conditions

The boundary conditions must be determined adequately and appropriately in order to obtain accurate results in FE programs. The calculation equations of possible axial tensile (T) and compressive  $(P_1)$  strengths in the case of a typical mechanism corresponding to the buckling moment of the brace members under the axial compressive force specified in Article 9.6 in TBEC (2019) [3] and illustrated in Fig. 8 are given in Eq. (1) and Eq. (2), respectively. The limit states were determined according to these equations.

$$T = R_{\nu} F_{\nu} A_{\alpha} \tag{1}$$

$$P_1 = 1.14 F_{cre} A_a \tag{2}$$

where  $R_y$  is the coefficient to calculate the possible strengths,  $F_y$  is the yield stress of the material,  $A_g$  is the gross gross area of the profiles and  $F_{cre}$  is the elastic critical buckling stress.

In the critical buckling stress calculation specified in Article 8.2 in SDCCSS (2018) [2], the yield stress was taken equal to the possible yield stress, and Eq. (3a) and Eq. (3b) were obtained to be used in the critical buckling stress calculation.

$$\frac{L_c}{i} \le 4.71 \sqrt{\frac{E}{R_y F_y}}, \qquad F_{cre} = \left[0.658^{\frac{R_y F_y}{F_e}}\right] R_y F_y \tag{3a}$$

$$\frac{L_c}{i} > 4.71 \sqrt{\frac{E}{R_y F_y}}$$
,  $F_{cre} = 0.877 F_e$  (3b)

where  $L_c$  is the critical buckling length, i is the radius of gyration of the profiles, E is the elasticity modulus of the material, and  $F_e$  is the elastic buckling stress.

In this study, since S275 structural steel and an outer diameter of 127 mm circular profile with 10 mm wall thickness are used, the gross cross-sectional area and the moment of inertia of the profile are obtained from Eq. (4) and Eq. (5), respectively. Additionally, the radius of gyration is calculated using Eq. (6). Since buckling coefficient K should be taken 1 as long as it is not proven by an approximation, the critical buckling length,  $L_c$ , can be defined as 6,000 mm.

$$A_g = \frac{\pi}{4}(D^2 - d^2) = \frac{\pi}{4}(127^2 - 107^2) = 3,675.66 \text{ mm}^2$$
 (4)

$$I = \frac{\pi}{64}(D^4 - d^4) = \frac{\pi}{64}(127^4 - 107^4) = 6,335,465 \text{ mm}^4$$
 (5)

$$i = \sqrt{\frac{I}{A_g}} = \sqrt{\frac{6,335,465}{3,675.66}} = 41.52 \text{ mm}$$
 (6)

where D and d are the outer and inner diameters, respectively, I is the moment of inertia, and i is the radius of gyration of the profiles.

According to Eq. (7), the elastic buckling stress is calculated as follows. The critical buckling stress is calculated using Eq. (3b) after checking the conditions.

$$F_{e} = \frac{\pi^{2}(200,000)}{\left(\frac{6,000}{41.52}\right)^{2}} = 94.51 \text{ N/mm}^{2}$$

$$4.71 \sqrt{\frac{E}{R_{y}F_{y}}} = 4.71 \sqrt{\frac{(200,000)}{(1.4)(275)}} = 107.35$$

$$\frac{L_{c}}{i} = \frac{6,000}{41.52} = 144.52 > 107.35$$

$$F_{cre} = 0.877(94.51) = 82.88 \text{ N/mm}^{2}$$

Finally, the possible axial tensile and compressive design strengths (forces) of the profiles are calculated using Eq. (1) and Eq. (2) and applied to the top surfaces of the tension and compression brace elements as well as the bottom surface of the compression member. The bottom surface of the tension profile was restrained using a pin support definition.

$$T = (1.4)(275)(3,675.66) = 1,415,130 \text{ N}$$
 (8a)

$$P_1 = (1.14)(82.88)(3,675.66) = 347,304 \text{ N}$$
 (8b)

Earthquake Direction

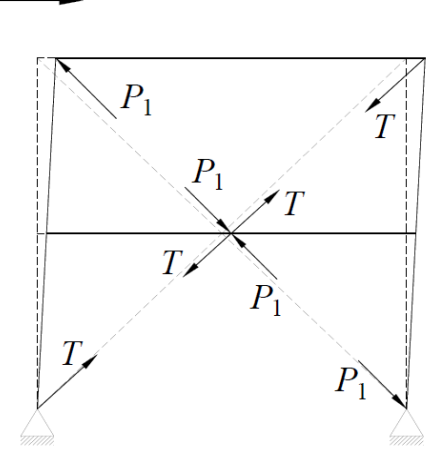


Fig. 8. Formation of possible tensile and compressive forces

## 3. Results and discussions

In the examinations of the analysis results, Von-Mises stresses were obtained along the members and the Paths in the models. The stress distributions on the profiles, the connection plate, and the weld are shown in Fig. 9. The highest stress values were obtained along the weld, especially at the endpoints, and on the surface of the tension profile. The center points of path-4 and path-8 were taken as reference points (0.00 mm) for each model and the distances of the points along the paths were shown with respect to the reference point. The points on the left were marked with a negative sign and those on the right were marked with a positive sign. In these paths, the total number of divided points (finite elements) along the cut surfaces is 79 points in between (-198.98 mm, 198.98 mm) distance, 69 points in between (-173.47 mm, 173.47 mm) distance, and 65 points in between (-163.27 mm, 163.27 mm) distance for each model with the intersection angles of 60°, 75°, and 90°, respectively. There is approximately a 5.1 mm distance between each point to obtain the stress results. In addition to these points, new points were defined along Path-4 and Path-8 from the end of the cut to the end of the middle part of the tension profile. In models with the intersection angles of  $60^{\circ}$ ,  $75^{\circ}$ , and 90°, there are 10 points between ( $\pm 198.98$  mm,  $\pm 250.00$  mm), 15 points between ( $\pm 173.47$  mm,  $\pm 250.00$ mm), and 17 points between  $(\pm 163.27 \text{ mm}, \pm 250.00 \text{mm})$ , respectively, and the distance between each point is approximately the same with the points along the cut surfaces. Path-5 is located in the center right after the end of the cut surface as shown in Fig. 7, and the total numbers of points along the path are 99 points between (198.98 mm, 250.00 mm), (173.47 mm, 250.00 mm), and between (163.27 mm, 250.00 mm), for each model respectively. The distance between the points is approximately 0.53 mm, 0.80 mm, and 0.91 mm for the models with angles of 60°, 75° and 90°, respectively.

The stress distributions along Path-4, Path-8, and Path-5 were examined depending on the angle between the braces and the changes in the weld thickness. In all graphs, the blue line, the red line, and the green line are used for models with 60°, 75°, and 90° angles, respectively. The stress values obtained along the paths for the model with a 60° angle were shown in Fig. 10(a), (b), and (c) depending on the weld thickness. The comparison was also made in Fig. 10(d) for all the paths. When Path-4 and Path-8 were examined along the cut, it was observed that the possible yield strength was not exceeded at any point in the model with 3.5 mm weld thickness, and the stress reached 387.80 MPa only at the -188.78 mm point in Path-4 for the model with 5 mm weld thickness (Fig. 10(a)). In Path-8, the stress reached the value of 394.61 MPa at the 188.78 mm point for the same model. In the model with 7 mm weld thickness, the stress reached 388.56 MPa only at the -188.78 mm point in Path-4 and 394.85 MPa at the 188.78 mm point in Path-8 (Fig. 10(b)).

Regardless of the weld thickness, it is seen that the stresses on Path-4 and Path-8 in all models decrease regularly starting from the center-left of the cut towards the center point, increase regularly along the cut from the center to the right, and show sudden ups and downs in other parts until the endpoints of the cut. The stresses decrease suddenly at the cut endpoints. In Fig. 10(c), the stress changes on the Path-5 in the 60° angle model were given depending on the weld thickness. The stress values exceeded the possible yield strength at every point along the path, increased suddenly formed a peak in the first 5 mm after the cut, and then suddenly decreased approximately at a distance of 5 mm after the peak. In all models, the stresses take their maximum values at the 202.72 mm point (approximately 5 mm after the end of the cut) and are 414.53 MPa, 414.57 MPa, and 412.71 MPa in the models with 3.5 mm, 5 mm, and 7 mm weld thickness, respectively.

When the stresses along all the paths are compared in Fig. 10(d), it is seen that the stresses in Path-5 give higher values than the other paths. In addition, when the stresses in Path-4 and Path-8 with the same weld thickness were examined, it was determined that the stress results on the left of the center showed differences, but the values on the right were similar. It is thought that the reason for this distribution can be the unsymmetrical connection between the plate and the tension profile.

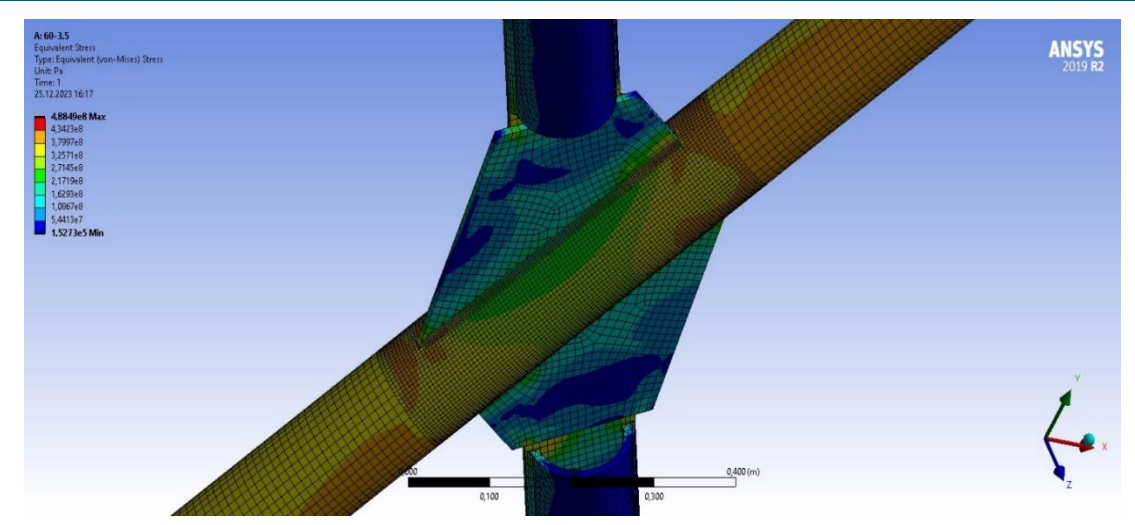


Fig. 9. Stress distribution in the members

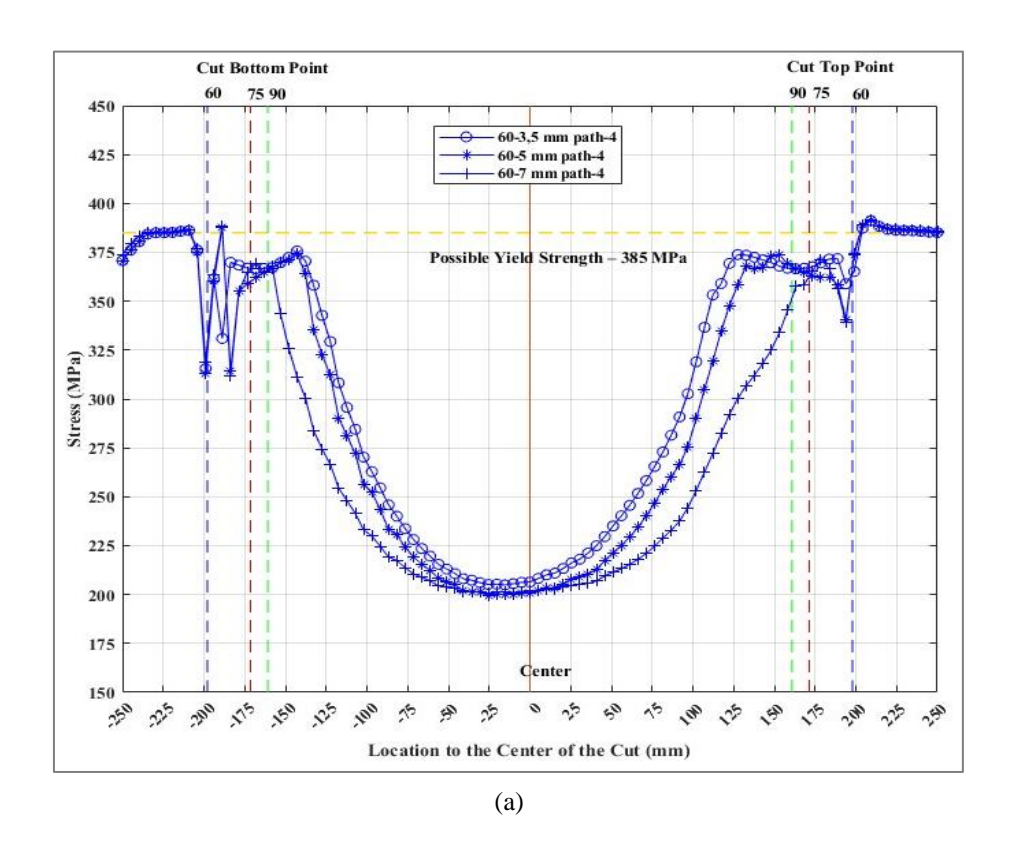
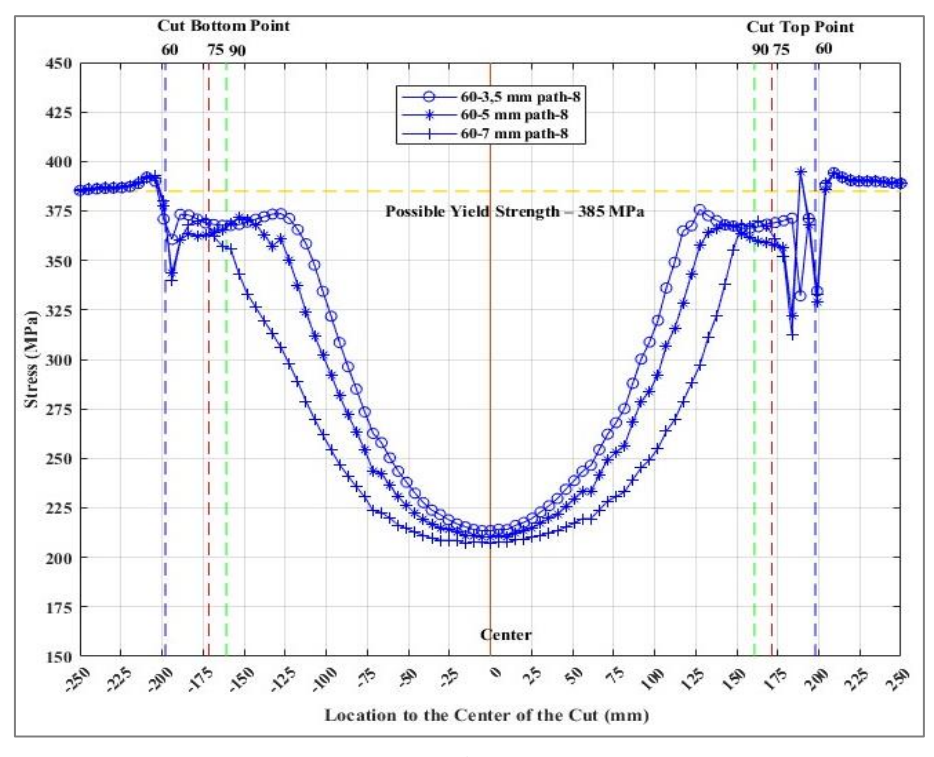
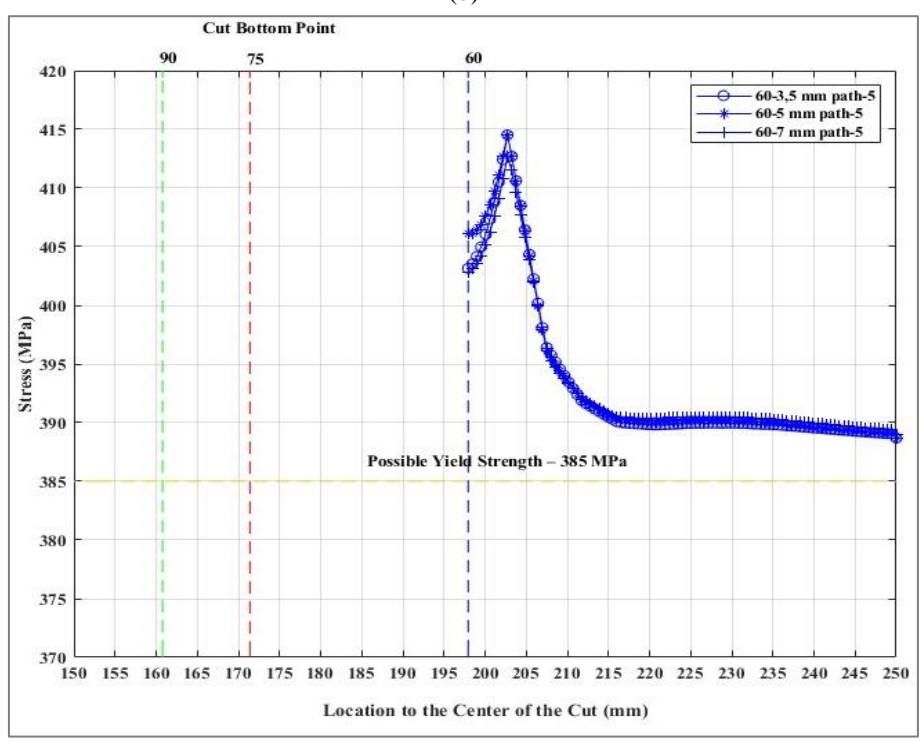


Fig. 10. Comparison of the models with 60° intersection angle (a) Path-4, (b) Path-8, (c) Path-5 (d) all paths



(b)



(c)

Fig. 10. Continued

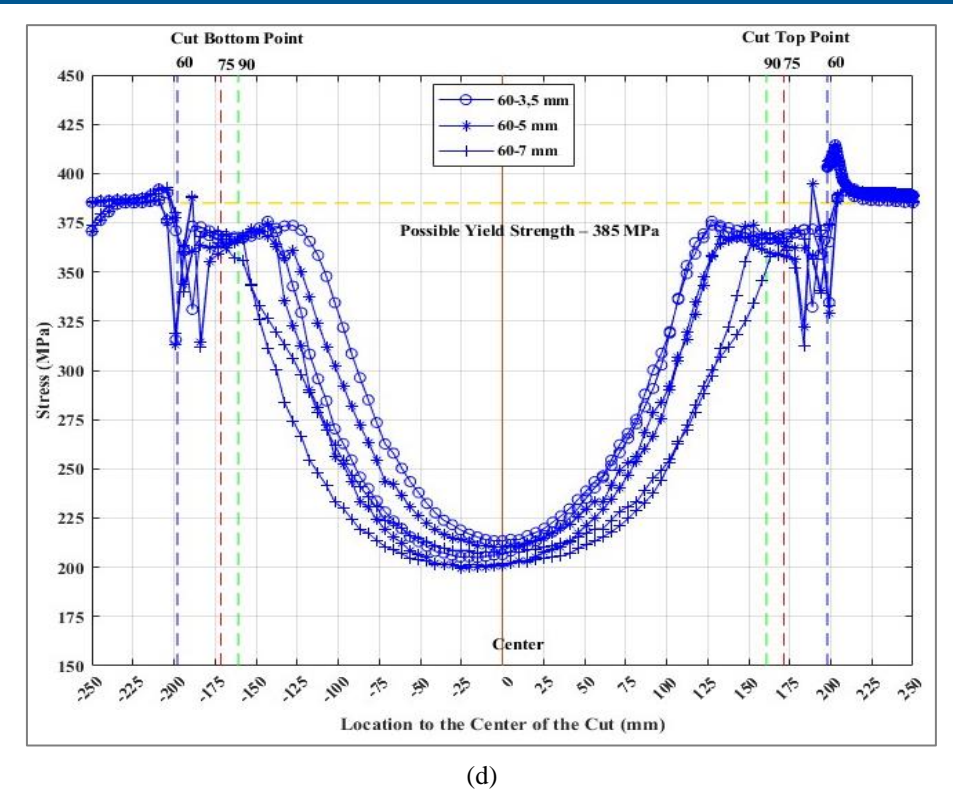


Fig. 10. Continued

In the model with an intersection angle of 75°, when Path-4 is examined along the cut, the yield strength is exceeded at 14 points in the ranges of (-153.06 mm, -132.65 mm) and (122.45 mm, 163.27 mm) for the model having a 3.5 mm weld thickness (Fig. 11(a)). The stress values vary between 385.06 MPa and 401.42 MPa along the ranges. In the model with 5 mm weld thickness, the stresses give higher values than the yield strength at 4 points in the ranges of (147.96 mm, 158.16 mm) and -153.06 mm points, and the values vary between 385.63 MPa and 400.01 MPa in these points. The yield strength is not exceeded at any point in the model with 7 mm weld thickness. Along Path-8, in the model with 3.5 mm weld thickness, the yield limit is exceeded at 19 points in the ranges of (-163.27 mm, -117.35 mm) and (112.24 mm, 153.06 mm), and the stress values vary between 385.22 MPa and 403.46 MPa in these ranges (Fig. 11(b)). The yield strength is exceeded at 7 points in the ranges (-158.16 mm, -142.86 mm) and (142.86 mm, 163.27 mm) for the model with 5 mm weld thickness, and the stress values vary between 385.58 MPa and 402.31 MPa in these ranges. In the model with 7 mm weld thickness, the stress magnitude is 387.93 MPa only at the 163.27 mm point and exceeds the yield limit.

As in the 60° angle models, the distribution of stresses in Path-4 and Path-8 follows the same behavior along the cut for the model with a 75° angle regardless of the weld thickness. In Fig. 11(c), it is seen that the stress changes on the Path-5 exhibit the same behavior with the model having an intersection angle of 60°. When all the results are compared in Fig. 11(d), it is found that the stresses in Path-5 give the largest values as in the 60° angle models. When the stresses in Path-4 and Path-8 with the same weld thickness were compared, it was found that the stresses in the 75° angle models showed the same behavior with the model having the intersection angle of 60° according to the center point.

In the model with an intersection angle of 90°, the changes in the stresses along Path-4, Path-8, and Path-5 depending on the weld thickness are shown in Fig. 12 (a), (b), and (c). The yield strength is exceeded at 13

points in the ranges of (-147.96 mm, -122.45 mm) and (117.35 mm, 147.96 mm) for the model having a 3.5 mm weld thickness along the Path-4 (Fig. 12(a)). The stress values vary between 385.05 MPa and 394.96 MPa along the points. In the model with 5 mm weld thickness, the stresses give higher values than the possible yield strength at 5 points, and the values are between 385.57 MPa and 397.73 MPa. The yield strength is not exceeded in the model with 7 mm weld thickness. Along Path-8, in the model with 3.5 mm weld thickness, the stresses at 16 points in the ranges of (-147.96 mm, -117.35 mm) and (107.14 mm, 147.96 mm) give higher results than the limit, and the stress values vary between 385.23 MPa and 402.99 MPa in these points (Fig. 12(b)). The stresses pass the yield strength at 4 points in the ranges of (137.76 mm, 147.96 mm) and the -147.96 mm point for the model with 5 mm weld thickness, and the stress values change between 385.36 MPa and 394.62 MPa. In the model with 7 mm weld thickness, the stress values are lower than the limit. In Fig. 12(c), it is observed that the stress changes on Path-5 exhibit the same behavior as the other models.

In addition, the stress distributions along the paths were studied depending on the angle between the brace elements. Figure 13 shows the results of models with 3.5 mm weld thickness. In Fig. 13(a), the smallest values of minimum and maximum stresses in the Path-4 were obtained in the 60° angle model. It was observed that the highest value of minimum stresses occurred in the 90° angle model and the highest value of maximum stresses was found in the 75° angle model. It is shown in Fig. 13(b) that the smallest value of minimum stresses was obtained in the 90° angle model and the highest value was obtained in the 60° angle model for the Path-8. The smallest of the maximum stress values occurs in the model with an angle of 60°, and the highest value was determined in the model with the intersection angle of 75°. When the stresses on Path-5 are evaluated, the smallest values of the minimum and maximum stresses occur in the model with a 90° angle, and the largest values are obtained in the model with a 60° angle. The stress values are above the yield limit.

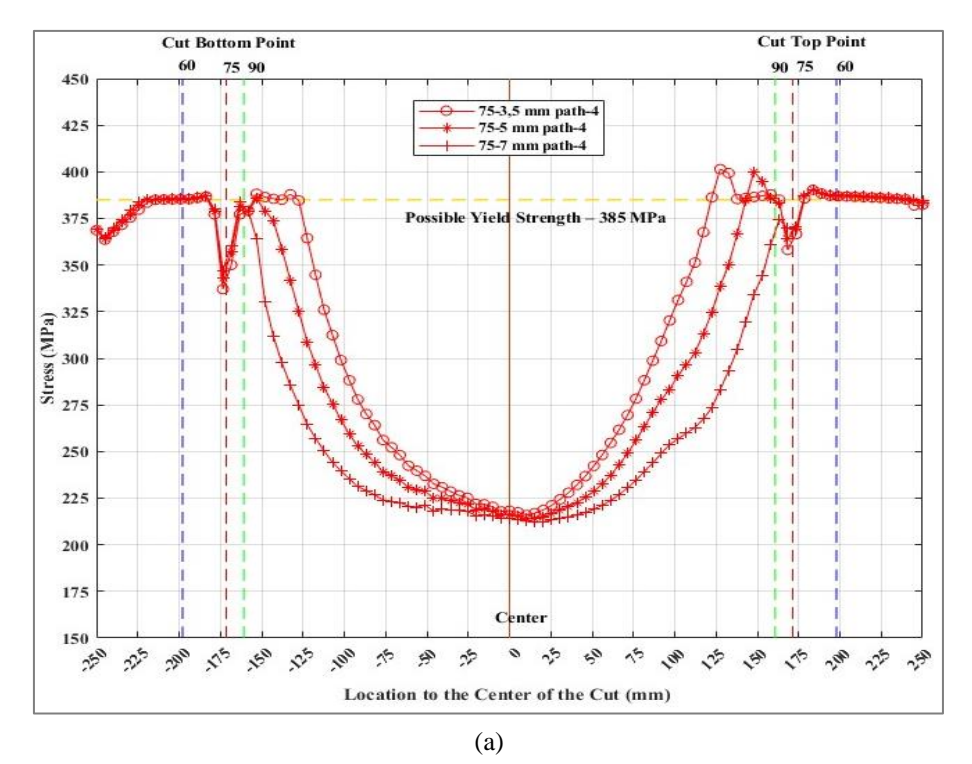
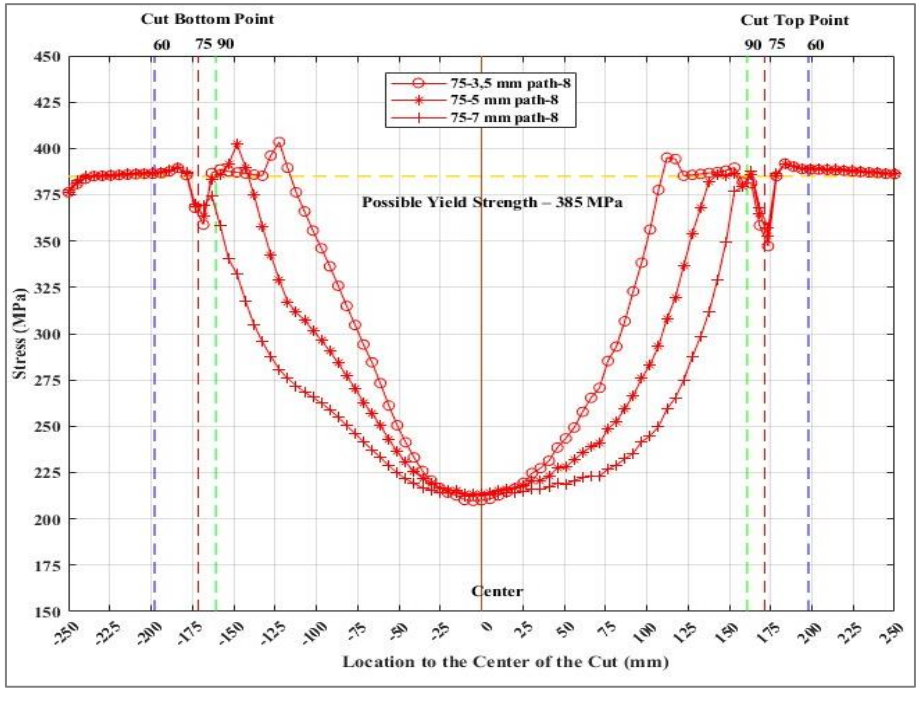
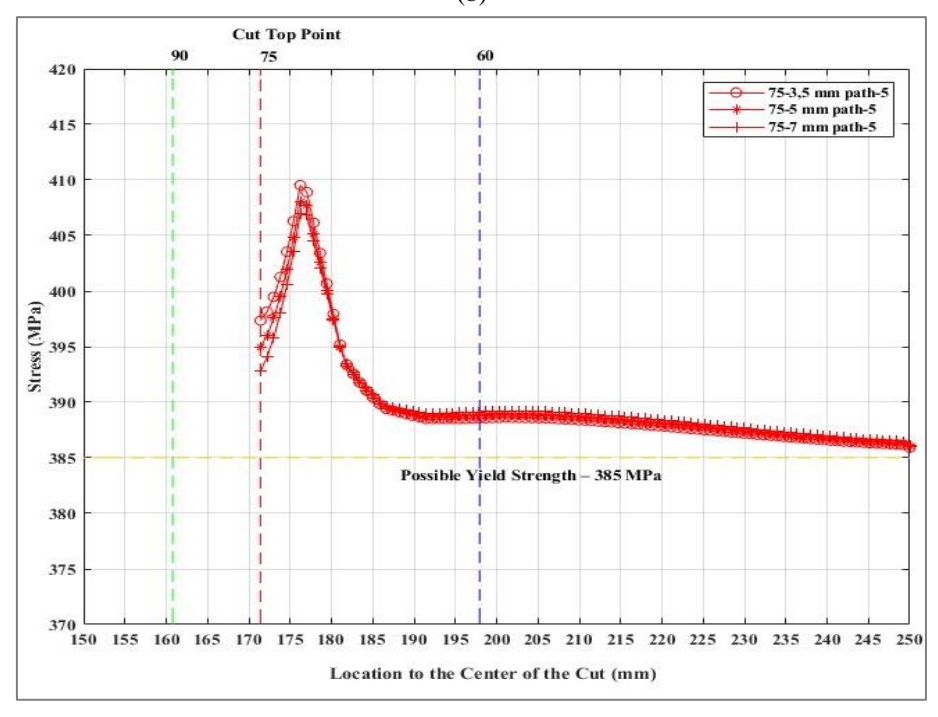


Fig. 11. Comparison of the models with 75° intersection angle (a) Path-4, (b) Path-8, (c) Path-5 (d) all paths



(b)



(c)

Fig. 11. Continued

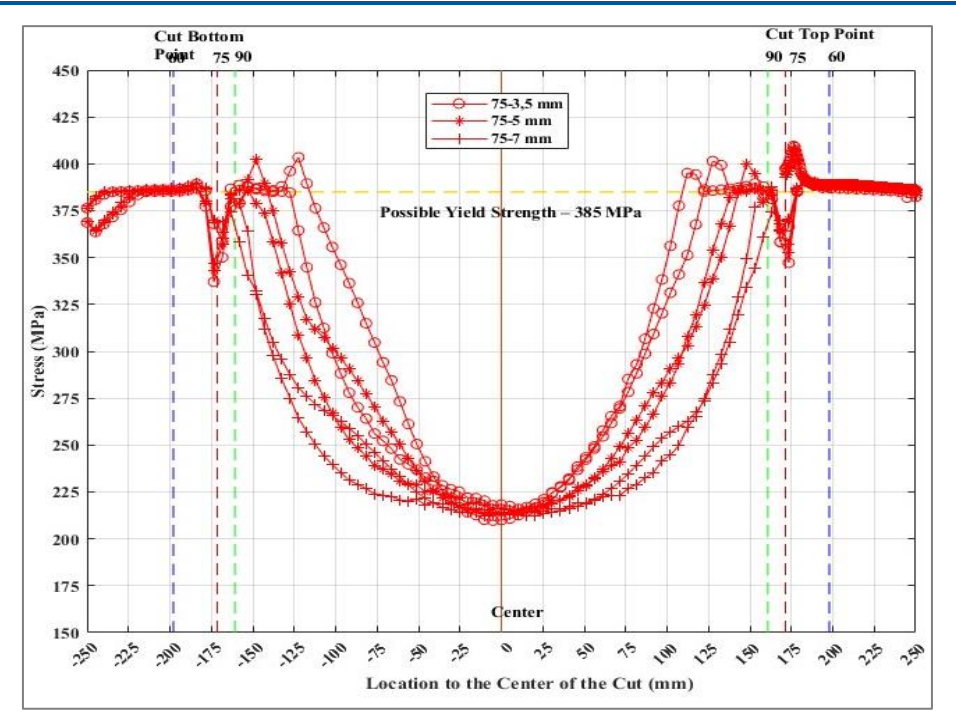


Fig. 11. Continued

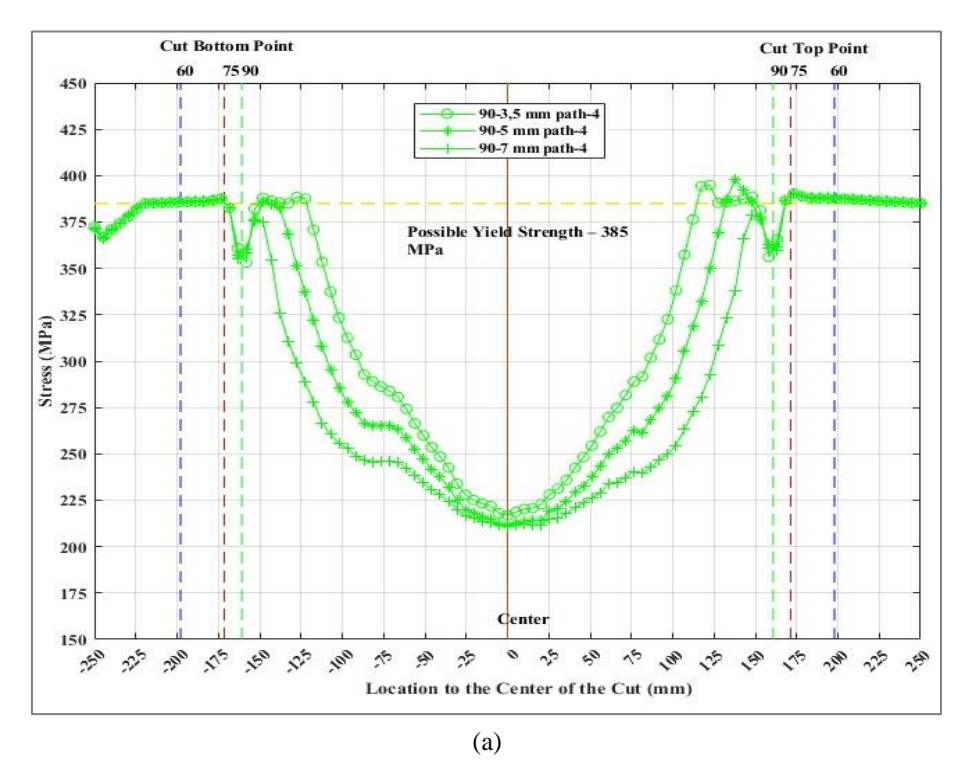
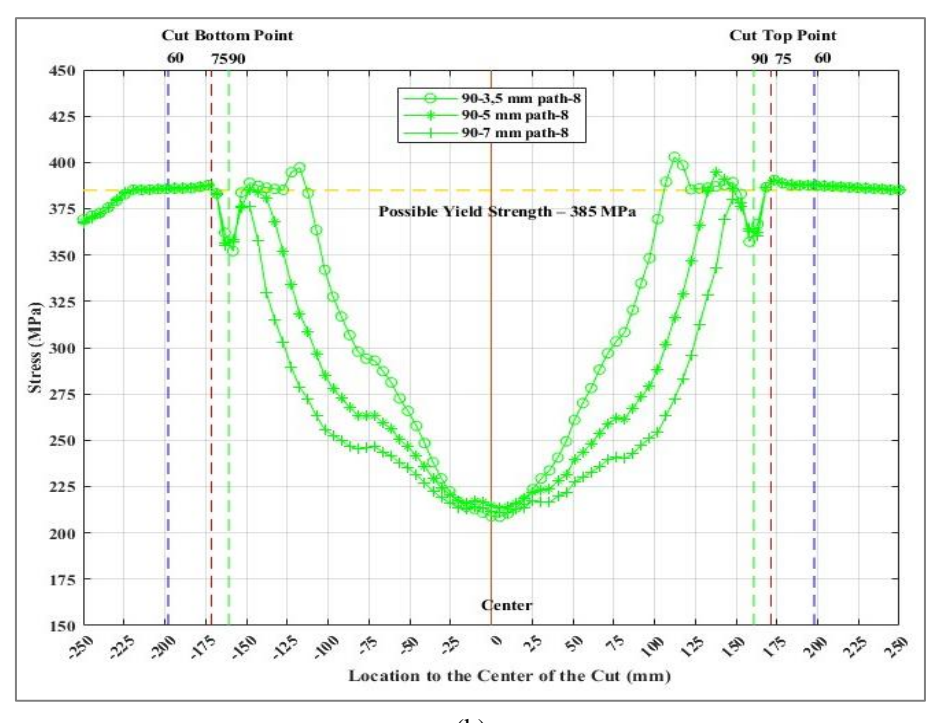


Fig. 12. Comparison of the models with 90° intersection angle (a) Path-4, (b) Path-8, (c) Path-5 (d) all paths



(b) Cut Top Point 420 90-3,5 mm path-5 90-5 mm path-5 415 90-7 mm path-5 410 405 Stress (MPa) 390 385 Possible Yield Strength - 385 MPa 380 375 370 150 155 160 165 170 175 180 185 190 195 200 205 210 215 220 225 230 235 240 245 250 Location to the Center of the Cut (mm)

(c) Fig. 12. Continued

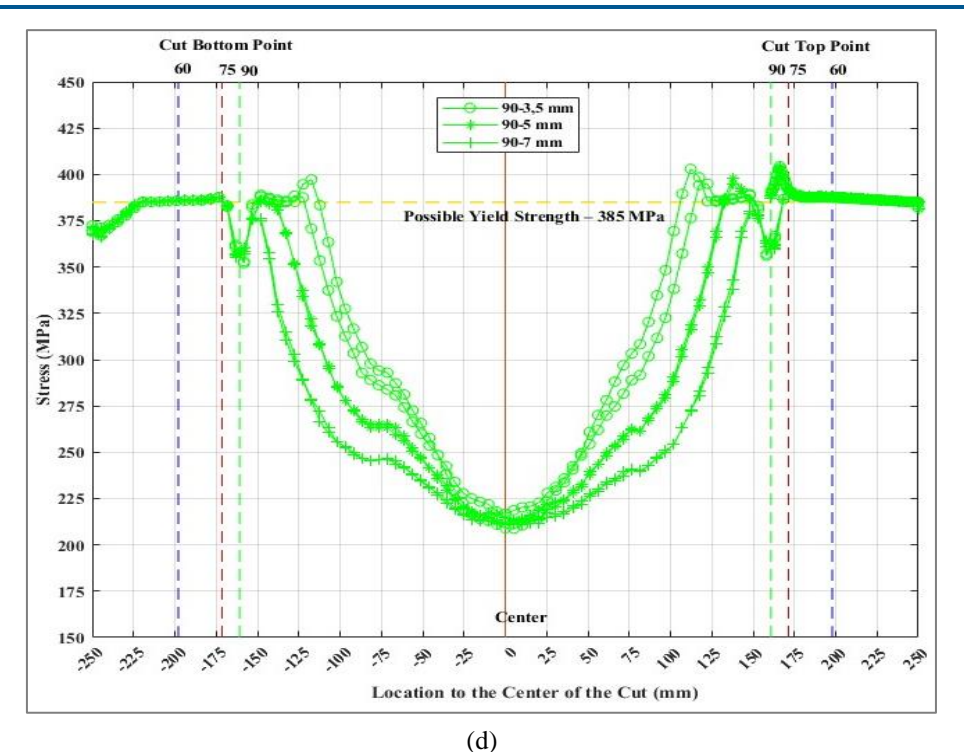


Fig. 12. Continued

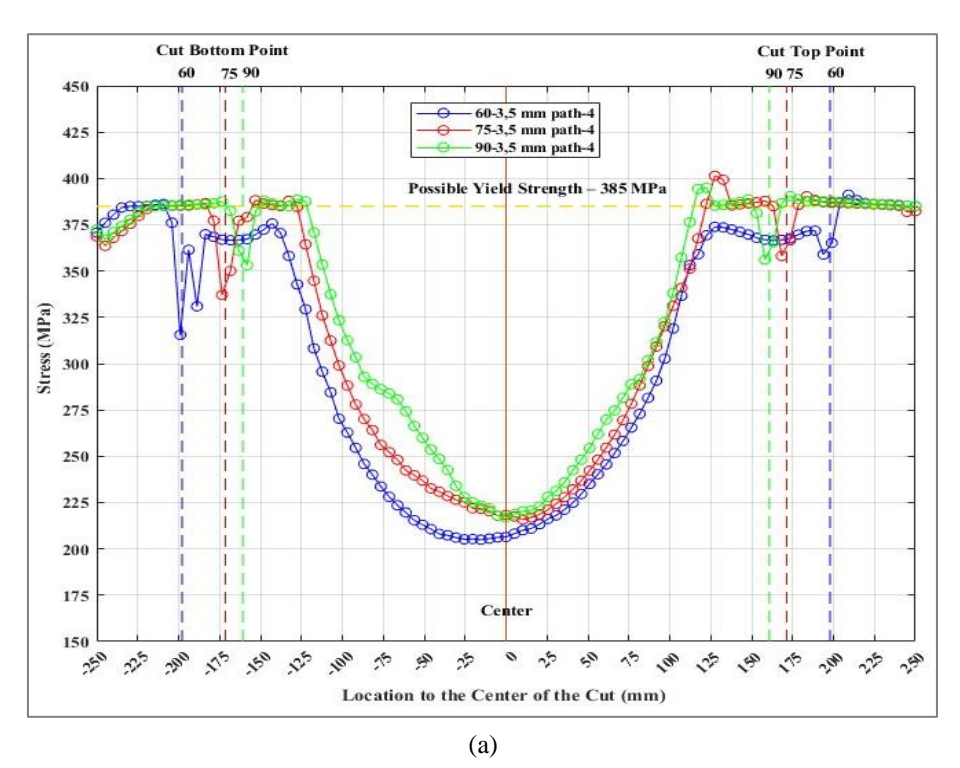
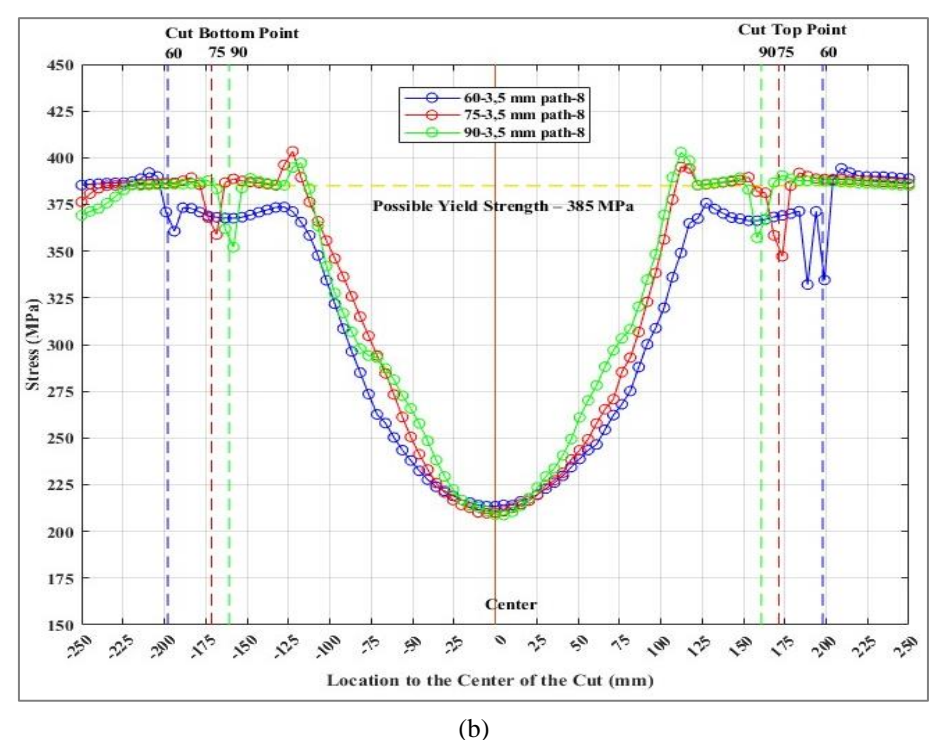
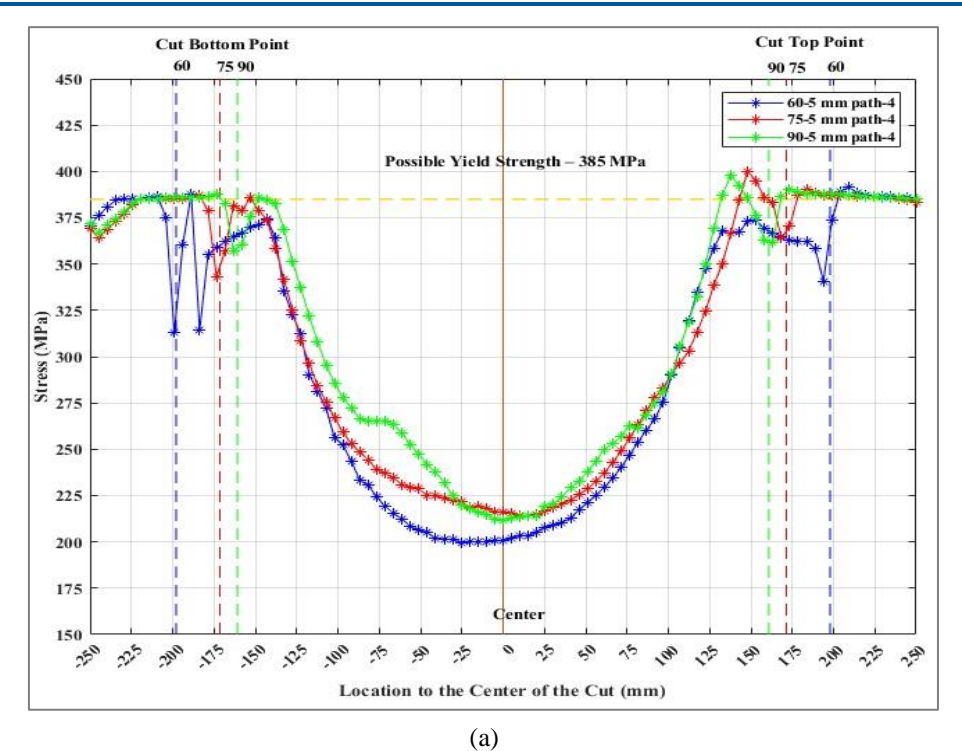


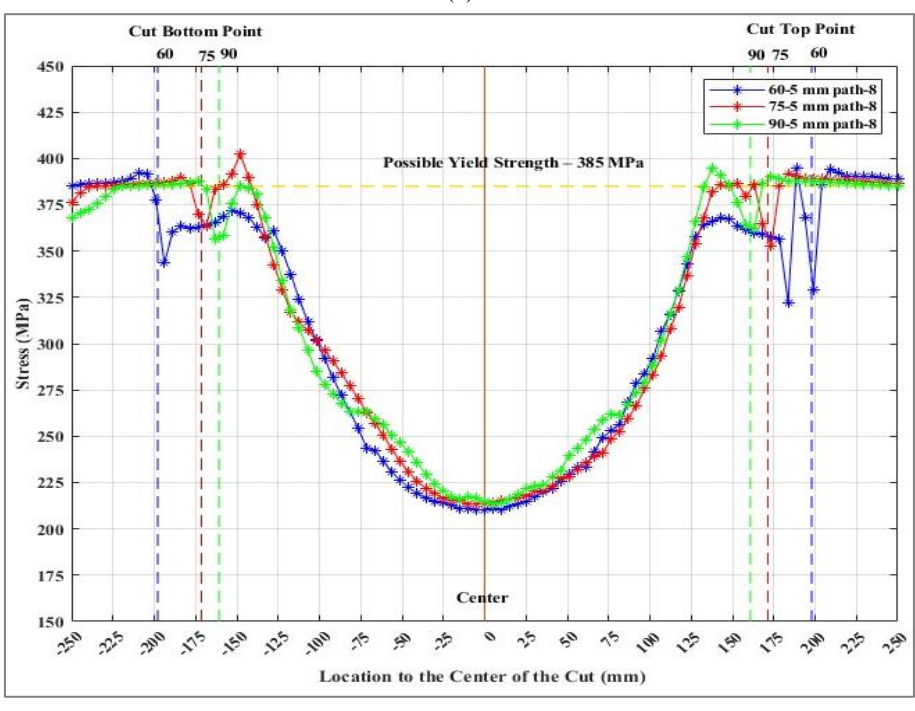
Fig. 13. Comparison of the models with 3.5 mm weld thickness (a) Path-4, (b) Path-8, (c) Path-5



**Cut Top Point** 60-3,5 mm path-5 75-3,5 mm path-5 90-3,5 mm path-5 Stress (MPa) Possible Yield Strength - 385 MPa Location to the Center of the Cut (mm)

(c) Fig. 13. Continued





(b) Fig. 14. Comparison of the models with 5 mm weld thickness (a) Path-4, (b) Path-8, (c) Path-5

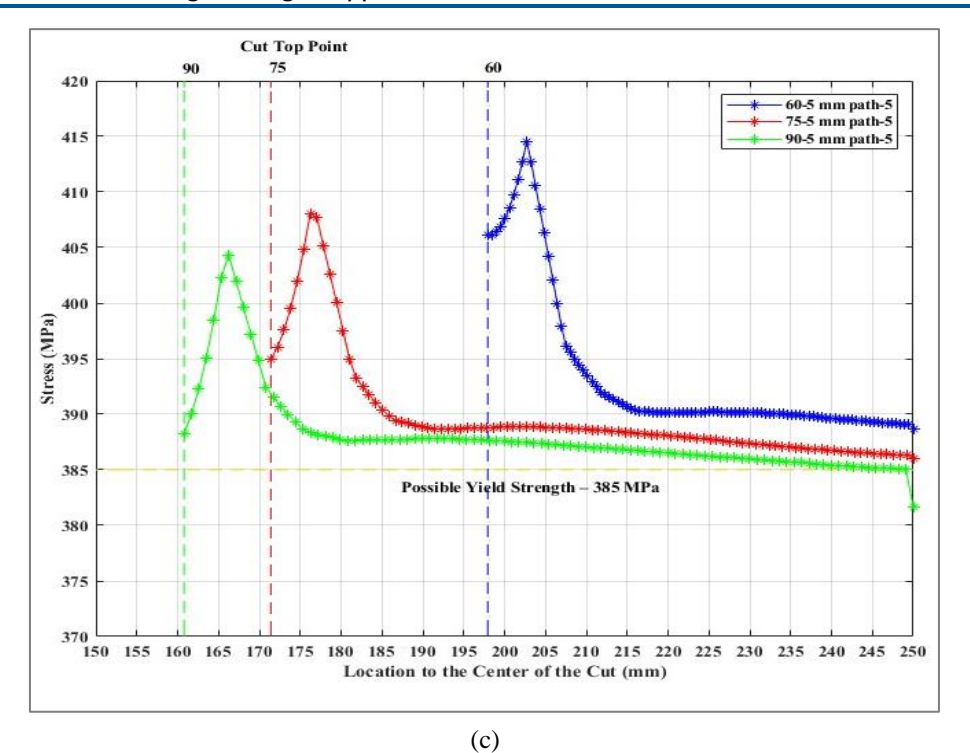


Fig. 14. Continued

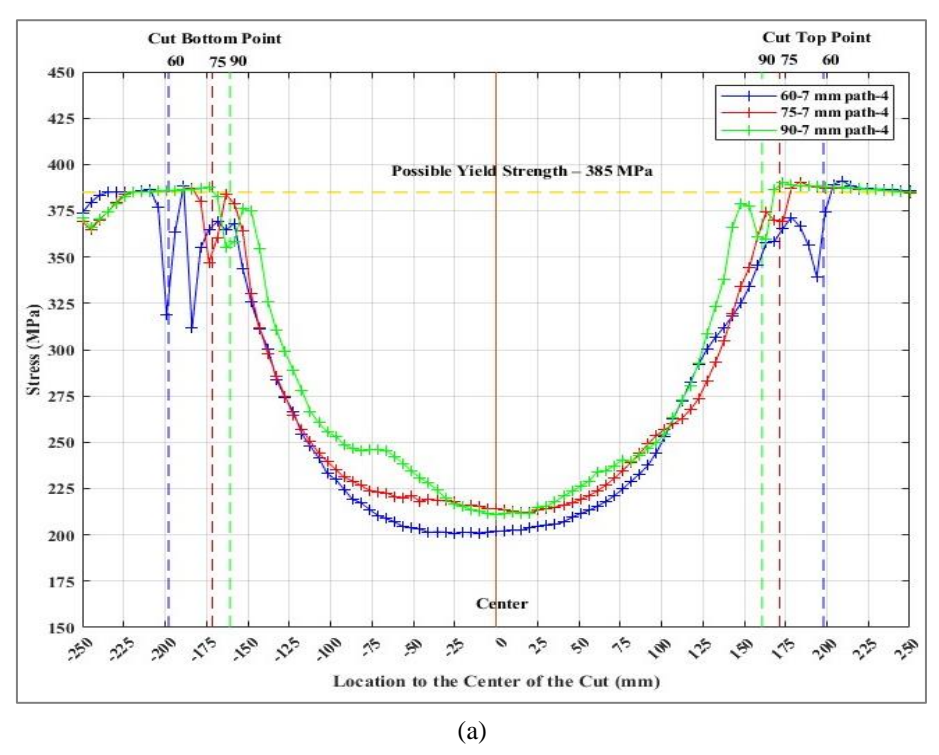


Fig. 15. Comparison of the models with 7 mm weld thickness (a) Path-4, (b) Path-8, (c) Path-5

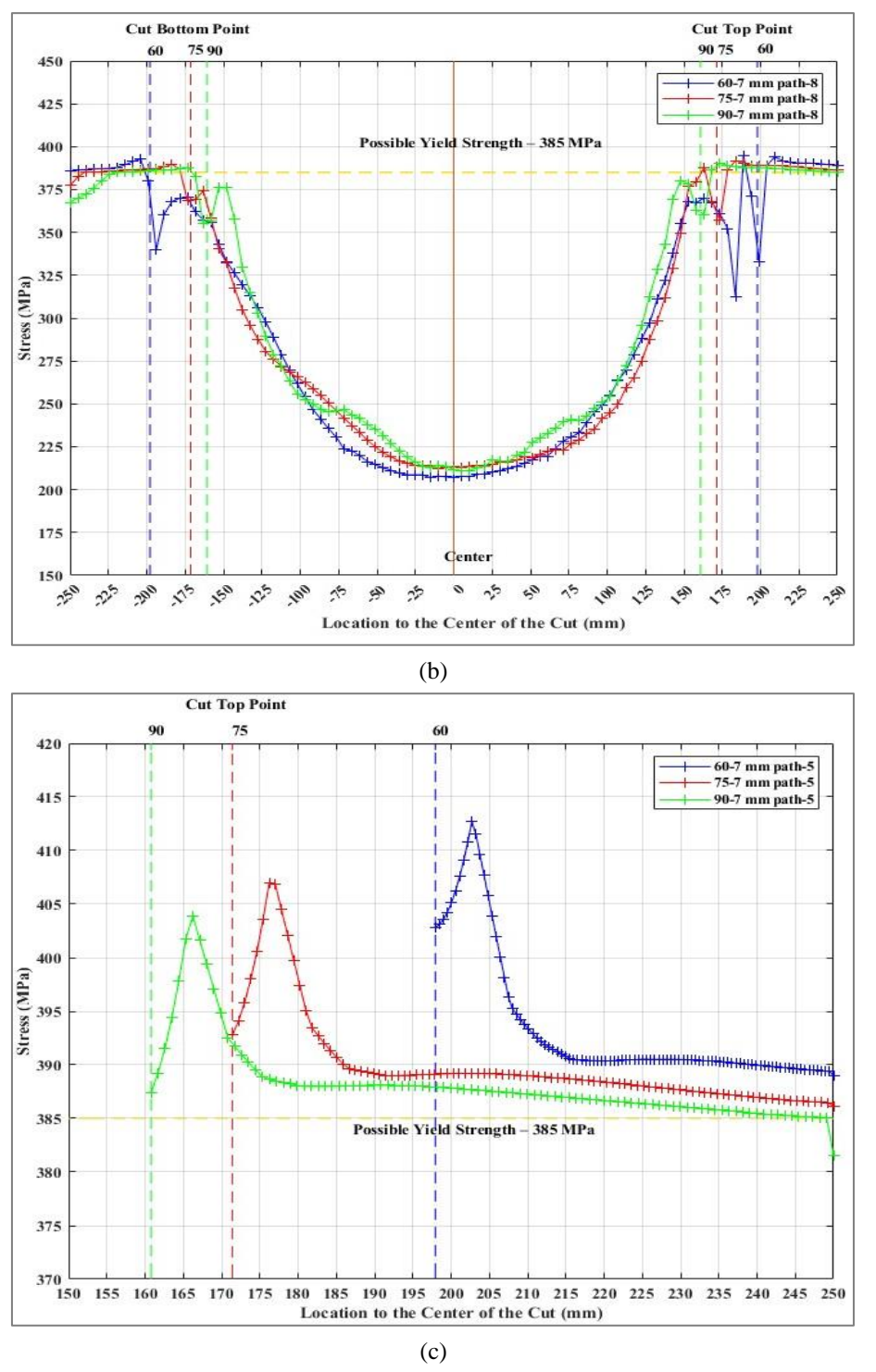


Fig. 15. Continued

Fig. 14 shows the results of models having 5 mm weld thickness. It is observed that the smallest values of minimum and maximum stresses in Path-4 occur in the 60° angle model (Fig. 14(a)), as in the model with 3.5 mm weld thickness. The highest values of the minimum and maximum stresses occur in the 75° angle

model. In Path-8, it is shown in Fig. 14(b) that the smallest values of minimum and maximum stresses were obtained in the 60° angle model. The smallest value of the maximum stress occurs in the model with the angle of 90°, and the largest value was in the model with the angle of 75°. It is shown in Figure 14(c) that the distribution of the stresses along Path-5 is almost the same as the models having 3.5 mm weld thickness.

The stress results of the models with 7 mm weld thickness are illustrated in Fig. 15. It is determined that the lowest value of the minimum stresses in Path-4 occurs in the 60° angle model, as in the earlier models. However, the highest value of the minimum stresses occurred in the 75° angle model as shown in Fig. 15(a). In Path-8, the smallest value of the minimum stresses is obtained in the 60° angle model and the largest in the 75° angle model (Fig. 15(b)). The smallest maximum stress values occur in the model with the 90° angle and the largest in the model with the 60° angle. When the stresses on Path-5 are compared, it is given in Fig. 15(c) that the results show the same behavior as in models with other weld thicknesses.

#### 4. Conclusions

Stress concentrations are investigated along the middle part of the tension profile due to the discontinuity in the profile cross-section of the X brace member, which is one of the elements used in the central steel braced frame systems. The angle between the brace elements and the weld thickness applied between the tension diagonal brace and the connection plate were changed and different models were defined in the ANSYS program. The following results were obtained from the FE analyses.

- 1. In all models, the regions where the highest stress values occur are along the direction of the tensile force in the tension profile and approximately at a distance of 5 mm after the end of the cut.
- 2. It has been observed that the thickness of the applied weld is not as effective as the angle change after the cut surface and the maximum stress value decreases if the intersection angle value between the braces increases from 60° to 90°.
- 3. It has been determined that the effect of the weld thickness on the maximum stress values along the cut decreases when the angle values between the braces increase from 60° to 90°.
- 4. In all models, it has been observed that the stress values suddenly drop below the possible yield strength value at the end of the cut surface towards the tensile direction due to the discontinuity between the cut and the tension profile.

In a further study, it is thought that the stress concentrations that may occur by changing the wall thickness of the profile and connection plate can be investigated.

#### Conflict of interests

The author(s) declared no potential conflicts of interest with respect to the research, authorship, and/or publication of this article.

# **Funding**

This research received no external funding.

## Data availability statement

Data generated during the current study are available from the corresponding author upon reasonable request.

#### References

[1] Durmuş G (2008) Experimental Investigation of Inelastic Torsional Response of Braced Steel Structures. Ph.D. Dissertation, Süleyman Demirel University.

[2] SDCCSS-2018 Specification for Design, Calculation and Construction of Steel Structures. Ministry of Environment, Urbanization, and Climate Change. <a href="https://www.resmigazete.gov.tr/eskiler/2018/02/20180215M1-4.htm">https://www.resmigazete.gov.tr/eskiler/2018/02/20180215M1-4.htm</a>, Ankara, Türkiye.

- [3] TBEC-2019 Turkish Building Earthquake Code. Ministry of Environment, Urbanization, and Climate Change. https://www.resmigazete.gov.tr/eskiler/2018/03/20180318M1-2.htm, Ankara, Türkiye.
- [4] Lekesiz İ (2016) The Effect of Bracing Type on Seismic Performance of a Typical Industrial Steel Structure. M.Sc. Thesis, Balıkesir University.
- [5] AISC, 2005. Seismic Provisions for Structural Steel Buildings. American Institute of Steel Construction, Inc. Chicago, Illinois.
- [6] Gül E (2022) Investigation of Stress Concentrations in Circular Cross Section X Diagonal Joints by Finite Element Method. M.Sc. Thesis, Yıldız Technical University.
- [7] Bosco M, Rossi P (2013) A design procedure for dual eccentrically braced systems: Analytical formulation. Journal of Constructional Steel Research 80:440-452.
- [8] Türker K, Lekesiz İ (2017) The effect of bracing type on seismic performance of a typical industrial steel structure. Dokuz Eylül University Faculty of Engineering Journal of Science and Engineering 19:821-834.
- [9] Dizdar O (2009) Seismic Performance of Concentrically Braced Frames. M.Sc. Thesis, Gebze Technical University.
- [10] Aşçı A (2012) Seismic Performance of Industrial Steel Buildings Designed by 2007 Turkish Earthquake Code. M.Sc. Thesis, Balıkesir University.
- [11] Bulut Y (2013) Effect of Brace Configuration on Dynamic Response of Special Braced Frames. M.Sc. Thesis, Gebze Technical University.
- [12] ANSYS Workbench User's Guide, Release 19.4, ANSYS, Inc., 2019.